Lateral Behaviour of Concrete-Filled FRP Tube Piles

Mostafa Jafarian Abyaneh, Hany El Naggar & Pedram Sadeghian
Department of Civil and Resource Engineering – Dalhousie University, Halifax, NS, Canada

ABSTRACT
Applications of fiber-reinforced polymer (FRP) composite piles are rapidly gaining traction in Canada and around the world. FRP piles offer several advantages compared to traditional piles, the most important of which is the corrosion resistivity and its applicability to marine applications or in any other corrosive environments. Concrete-filled FRP tube piles are the most commonly used type of these composite piles. In this system, there are two main structural components: an FRP shell or tube, and a concrete infill without steel reinforcement. The relative stiffness of these two components controls the piles performance to vertical and lateral loads. This paper investigates the effect of the relative stiffness of the individual pile's components on its structural and geotechnical performance utilizing 3D finite element models of a full-scale field tests conducted during the construction of route 40 Highway Bridge in Virginia. Based on the curves of deflection along the length of the pile, the modeling results were in good accordance with the experimental data, which means that the proposed model can be used in a parametric study to optimize the design of composite piles.

1 INTRODUCTION

Safety, durability and low maintenance of bridge structures are of great interest to civil engineers and governments. Failure of a bridge component due to corrosion can result in the collapse of the entire structure, especially when it occurs in the foundation. The replacement of corroded piles is difficult and expensive because of the superstructure resting on them. In recent years, North American highway agencies and researchers have started to investigate the viability of protecting bridge piles with anti-corrosive materials such as Fiber Reinforced Polymer (FRP) laminates (Roddenberry et al. 2014).

The FRP laminate used in structural piles is composed of several layers of fibers saturated with a polymeric resin. Different orientation of fibers with respect to the longitudinal axis of pile is often used in foundation piles resulting in higher stiffness and strength. The FRP tube contributes to the stiffness and strength in two ways: First, the circumferential stiffness of FRP provides confinement to the concrete core leading to higher strength and ductility of the pile. Second, the strength and stiffness of FRP laminate in the axial direction provides additional flexural strength for the structural pile (Kaw 2005).

Many bridge foundations in United States and Canada are subjected to harsh marine environments, which can cause expensive maintenance problems and shortened bridge life. Particularly, prestressed concrete pile foundations degrade rapidly when their prestressing steel strands corrode. In order to overcome this issue that happened for the old Route 40 Bridge in Virginia, Fam et al. (2003) investigated the mechanical behavior of precast composite piles composed of concrete-filled FRP tubes in comparison to the conventional prestressed concrete piles. However, no numerical modeling has been conducted on the experimental results obtained from field testing of piles in the aforementioned study.

In this research, the mechanical behavior of precast concrete-filled FRP composite piles used in the construction of new Route 40 Bridge in Virginia (Fam et al. 2003) has been numerically modeled under different loading conditions. The range of applied loads modeled in this research ranges from 11 kips to 27 kips (49 kN to 120 kN). As a result, an advanced numerical model based on nonlinear finite element analysis (NFEA) was developed to predict the lateral deflection of composite pile. The failure criterion and damage model used in the modeling were based on Mohr-Coulomb plasticity model and disturbed state concept (DSC), respectively. This paper presents the results of the initial phase of a comprehensive study to optimize the design of composite piles.

2 MODELING

An advanced numerical model based on DSC damage model and Mohr-Coulomb failure criterion was developed to predict lateral deflection of composite pile considering its softening behavior under various lateral loading conditions. The values of applied lateral load modeled in this research are 11, 18, 21 and 27 kips. The interface of concrete, FRP and confining soil has also been investigated in the proposed model.

2.1 Experimental test setup

The composite piles used in the new Route 40 Bridge in Virginia (Pando et al. 2006) are composed of concrete-filled circular glass FRP (GFRP) tubes. The volume ratio of fibers in the tube is 51 percent. The outer diameter and net structural wall thickness of the GFRP tube are 24.6 inches (625 mm) and 0.213 inches (5.41 mm), respectively. The length of the composite pile is 43 ft (13.1 m), and the point of lateral load application was approximately 3 m (9.84 ft) above the ground surface for the composite pile. More details about the experiment can be found in Fam et al. (2003) and Pando et al. (2006).

2.2 Disturbed state concept (DSC)

The fundamental idea behind the applied model is based on the DSC damage model, which can be formulated as decomposition of material behavior into its relatively intact (RI) and fully adjusted (FA) components. A schematic illustration of the DSC has been shown in Figure 1. As can be seen in the figure, the blank and solid areas represent the RI and FA parts, respectively. The initial response of material is absolutely RI without any visible cracks. As applied displacement increases, the FA response becomes more predominant with propagation of cracks resulting in completely FA behavior at the failure of corresponding specimen. Based on the concept proposed by Desai (2000), the disturbance can be defined as:

$$D = D_u(1 - e^{-A\zeta_D^Z}) \quad [1]$$

where D_u is the ultimate value of disturbance; A and Z are material parameters; and ζ_D is the trajectory of deviatoric plastic strain as follows:

$$\zeta_D = \int (d\mathbf{E}_{ij}^p d\mathbf{E}_{ij}^p)^{\frac{1}{2}} \quad [2]$$

where E_{ij} represents the deviatoric strain tensor of the total strain tensor ε_{ij}. The disturbance of stress-strain curve can be generally expressed as:

$$D = \frac{\sigma^{RI} - \sigma^{obs}}{\sigma^{RI} - \sigma^{FA}} \quad [3]$$

where σ^{RI}, σ^{FA}, σ^{obs} are relatively intact (RI), fully adjusted (FA), and observed stresses, respectively. In the presented model, this definition was also used for volumetric strain versus strain curve. In order to find the A and Z parameters, (1) and (3) were equated for two arbitrary points of experimental curve. The disturbance parameters (A, Z, and D_u) were used for predicting experimental behavior of independent tests of the same material. The dependence of RI and FA states is different in the modeling procedure. The modulus of elasticity and the type of epoxy resin affect the RI behavior, while the confining conditions and residual strength control the FA behavior. After determination of disturbance parameters for each specimen, stress increments can be obtained by using following equation (Desai 2015):

$$d\sigma_{ij} = (1 - D)C_{ijkl}^{ep} d\varepsilon_{kl} + \frac{D}{3}\delta_{ij}C_{ppkl}^{ep} d\varepsilon_{kl} - dD(\sigma_{ij}^{RI} - \sigma_{ij}^{FA}) \quad [4]$$

In the pre-failure stage where D = 0, Eq. 4 represents RI state. The RI response can be predicted by using different models from simple mathematical models to advanced models such as the HISS plasticity model. In this study, NFEA and HISS δ_0 plasticity model have been utilized in order to predict the RI response.

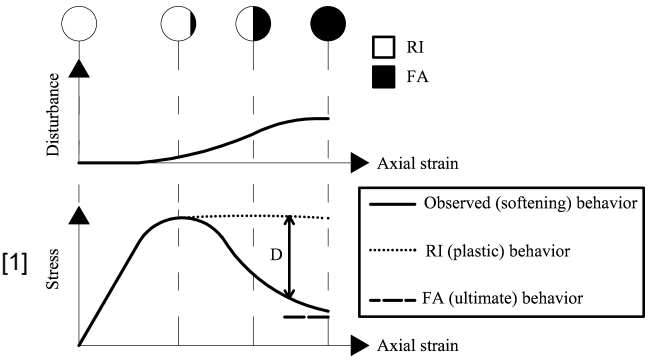

Figure 1. Schematic representation of DSC decomposition

2.3 Mohr-Coulomb failure criterion

The Mohr–Coulomb (M–C) plasticity model allows for the effect of friction and interface problems. The corresponding yield surface plots as an irregular hexagon in the principal stresses space. One of the most important characteristics of this criterion is that it can provide different strengths under various paths of stress or loading, for instance: compression, simple shear, and extension. Consequently, this failure criterion is often considered to be more appropriate for frictional and geologic materials. The yield function of Mohr-Coulomb failure criterion can be written as (Labuz and Zang 2012):

$$F = J_1 \sin\phi + \sqrt{J_{2D}}\cos\theta - \frac{\sqrt{J_{2D}}}{3}\sin\phi\sin\theta - c\cos\phi \quad [5]$$

where J_1 and J_{2D} are the first invariant of stress and second invariant of deviatoric stress, respectively. The parameters c and ϕ are cohesion and angle of friction of Mohr-Coulomb failure criterion. θ is the Lode angle which can be written as:

$$\theta = \frac{1}{3}\sin^{-1}\left(-\frac{3\sqrt{3}}{2}\frac{J_{3D}}{J_{2D}^{3/2}}\right) \quad [6]$$

where J_{3D} is the third invariant of deviatoric stress. The value of θ must be acquired in the range of $[-\pi/6, \pi/6]$ (Desai 2000).

2.4 Proposed model

As it can be seen in Figure 2, the initial steps in developing the model was defining the geometry of the problem, number of steps, elastoplastic parameters and Gaussian points for initial interpolation and final extrapolation of stress and strain values. By generating a finite element method (FEM) mesh, nodal freedom and loads can be determined.

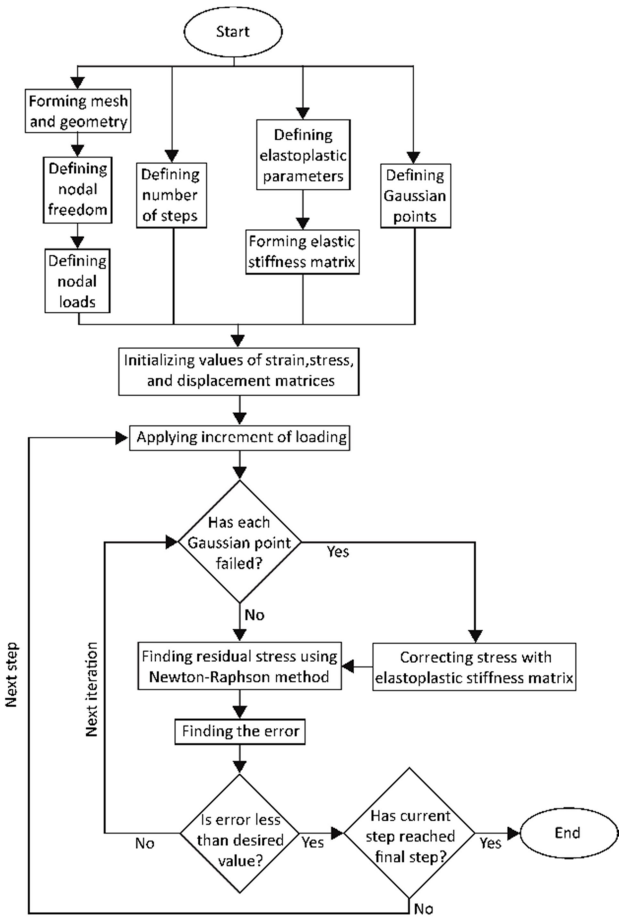

Figure 2. Flowchart of the proposed NFEA model

Since the applied load and geometry of specimens are axisymmetric, all quantities of interest in structural analysis including displacements, strains, and stresses are independent of the circumferential coordinate (Khoei 2005). Therefore, a plane whose width and length are radius and height of cylindrical composite pile was modeled instead of modeling the whole pile as depicted in Figure 3.

For implementation of NFEA, a FEM mesh was generated for the concrete-filled FRP composite pile as shown in Figure 4. As can be seen in the figure, the interface of concrete, FRP laminate and soil was addressed by the blank elements between soil and concrete. Moreover, the friction and normal stress of the soil with FRP and concrete were considered in the aforementioned interface elements.

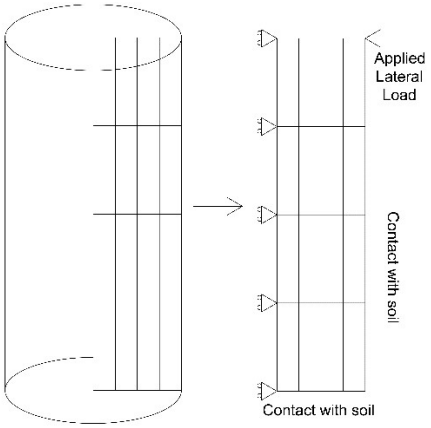

Figure 3. The schematic configuration of generated mesh for axisymmetric cylinder.

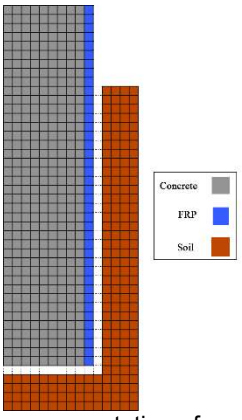

Figure 4. Schematic representation of generated mesh for the interface of concrete, FRP laminate and soil in the proposed model.

Afterwards, the values of strain, stress, and displacement matrices were initialized. By applying the first increment of loading, the failure of each Gaussian point was checked. If the Gaussian point has failed, the elastic prediction has to be corrected with elastoplastic stiffness matrix. In order to satisfy the equilibrium conditions between internal and external forces, the norm of following residual stress ($\boldsymbol{\psi}$) must approach zero through required iterations (Khoei 2005):

$$\boldsymbol{\psi} = \int_V \bar{\mathbf{B}}\boldsymbol{\sigma} d_V - \mathbf{F} \quad [7]$$

where V is the volume of the specimen, **F** represents external forces tensor, **σ** is the Cauchy stress tensor, and $\bar{\mathbf{B}}$ is the tensor relating the increments of strain and displacement ($\Delta\boldsymbol{\varepsilon} = \bar{\mathbf{B}}\Delta\bar{\mathbf{u}}$). In order to find the value of stress in each step of loading, the increment of stresses can be expressed as:

$$\begin{Bmatrix} \Delta\boldsymbol{\sigma}_r \\ \Delta\boldsymbol{\sigma}_\theta \\ \Delta\boldsymbol{\sigma}_z \\ \Delta\boldsymbol{\sigma}_{rz} \end{Bmatrix} = \mathbf{C} \begin{Bmatrix} \Delta\boldsymbol{\varepsilon}_r \\ \Delta\boldsymbol{\varepsilon}_\theta \\ \Delta\boldsymbol{\varepsilon}_z \\ \Delta\boldsymbol{\gamma}_{rz} \end{Bmatrix}$$

where **C** is the stiffness matrix, which can be elastic ($\mathbf{C}_e$) or elastic-plastic ($\mathbf{C}_{ep}$) depending on whether the corresponding Gaussian point has yielded or not. The indices *r*, *θ*, and *z* represent radial, angular, altitudinal components of stress and strain. Elastic-plastic stiffness matrix can be expressed as (Akhaveissy et al. 2009):

$$\mathbf{C}_{ep} = \mathbf{C}_e - \frac{\mathbf{C}_e \mathbf{n}\mathbf{n}^T \mathbf{C}_e}{H + \mathbf{n}^T \mathbf{C}_e \mathbf{n}}$$

where H is the hardening modulus, n is the flow rule vector that shows growth direction of the failure surface.

3 RESULTS AND DISCUSSION

Lateral load tests were applied on the composite piles, using the Statnamic Testing System as described in Pando et al. (2006). The loading system was placed horizontally in order to apply a lateral load on the top of the composite pile. According to the aforementioned test results, several measurements were obtained during the Statnamic test. These measurements include the lateral displacement for each value of applied load to the composite pile at different depths. Four loading cycles were considered for the composite piles by increasing the applied load.

The values of the lateral deflection distribution along the length of the composite pile at the peak load for each of the four loading cycles were extracted from the test results (Fam et al. 2003) to verify the parameters of the proposed model. The lateral deflection versus depth below the load point for 11, 18, 21 and 27 kips has been shown in Figure 5, 6, 7 and 8, respectively. As can be seen in the figures, the lateral deflections become insignificant at a certain depth of about 15 ft (4.5 m) from the loading point. The change of the slope is related to the failure of composite pile as well as soil.

[8

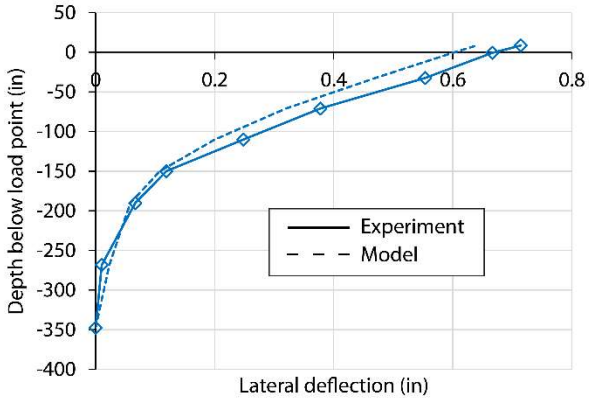

Figure 5. Lateral deflection along the length of composite pile under 11 kips lateral loading.

[9

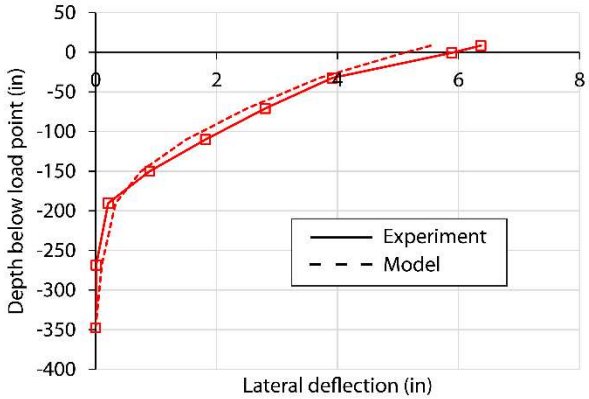

Figure 6. Lateral deflection along the length of composite pile under 18 kips lateral loading.

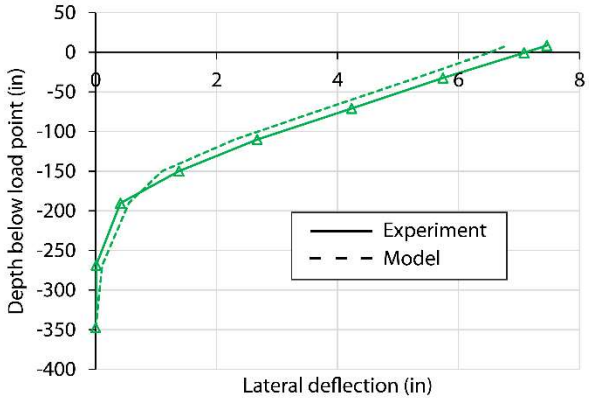

Figure 7. Lateral deflection along the length of composite pile under 21 kips lateral loading.

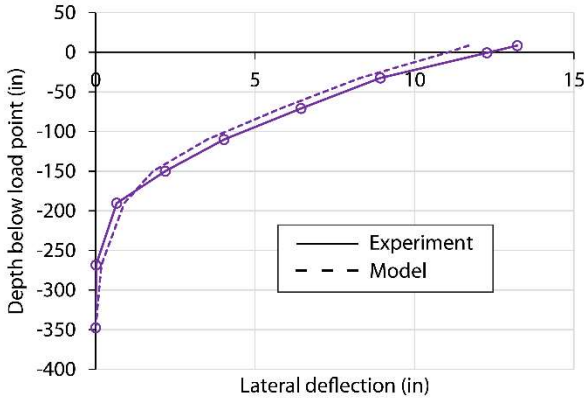

Figure 8. Lateral deflection along the length of composite pile under 27 kips lateral loading.

More details regarding the layers of the confining soil have been depicted in Figure 9 (Pando et al. 2006). As it can be seen in the figures, the lateral deflection becomes infinitesimal from the point soil structure changes from medium dense sand to very stiff to hard clay regardless of the magnitude of loading. By comparing the results, it can be concluded that the numerical results obtained from the proposed model are in good accordance with the experimental data.

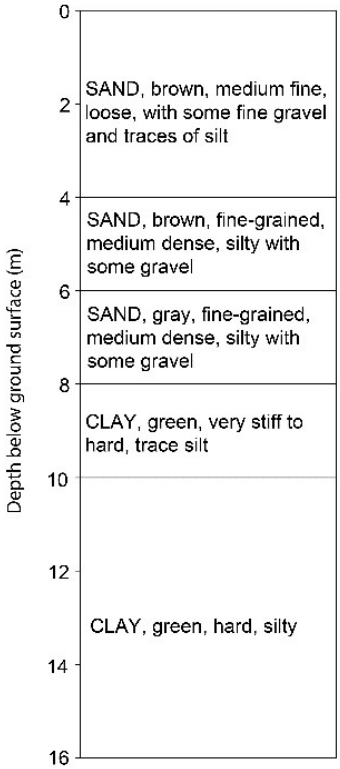

Figure 9. Schematic representation of soil layers at the bridge site (Pando et al. 2006).

4 CONCLUSIONS

In this paper, an advanced nonlinear finite element model based on disturbed state concept (DSC) damage model and Mohr-Coulomb failure criterion was proposed to predict the mechanical behavior of concrete-filled FRP tube pile. Furthermore, the interface of concrete, FRP laminate and soil was modeled and the results were obtained. The nonlinearity used in the model was composed of both material and geometry nonlinearity. The curves of lateral deflection versus depth below the applied load were used to verify the accuracy of the developed model. The modeling results showed good agreement with the experimental data, which means that the proposed model can be used to predict the mechanical behavior of bridge composite piles with an acceptable accuracy. It is worth noting that this is an ongoing research and more results will be presented at the time of the conference. Moreover, a comprehensive parametric study is underway to optimize the design of composite piles and investigate the effects of various key parameters on its soil structure interaction (SSI) behavior.

5 REFERENCES

Akhaveissy, A.H., Desai, C.S., Sadrnejad, S.A.A.D. and Shakib, H. 2009. Implementation and comparison of a generalized plasticity and disturbed state concept for the load-deformation behavior of foundations, *Scientia Iranica, Transaction A: Civil Engineering*, 16(3): 189-198.

Desai, C.S. 2000. *Mechanics of materials and interfaces: The disturbed state concept*, CRC press, Boca Raton, FL, United States.

Desai, C.S. 2015. Constitutive modeling of materials and contacts using the disturbed state concept: Part 1 – background and analysis, *Computers & Structures*, 146: 214-233.

Fam, A., Pando, M., Filz, G. and Rizkalla, S. 2003. Precast Piles for Route 40 Bridge in Virginia Using Concrete Filled FRP Tubes, *PCI Journal*, 48(3): 32-45.

Kaw, A.K. 2005. *Mechanics of composite materials*, 2nd ed., CRC press, Boca Raton, FL, United States.

Khoei, A.R. 2005. *Computational Plasticity in Powder Forming Processes*, Elsevier, Oxford, UK.

Labuz, J.F. and Zang, A. 2012. Mohr-Coulomb Failure Criterion, *Rock Mechanics and Rock Engineering*, 45(6): 975-979.

Pando, M.A., Ealy, C.D., Filz, G.M., Lesko, J.J. and Hoppe, E.J. 2006. A Laboratory and Field Study of Composite Piles for Bridge Substructures, *Federal Highway Administration*, McLean, VA, United States.

Roddenberry, M., Mtenga, P. and Joshi, K. 2014. Investigation of Carbon Fiber Composite Cables (CFCC) in Prestressed Concrete Piles, *Transportation Research Board*, Washington, DC, United States.